JOURNAL OF AIRCRAFT
Vol. 39, No. 5, September–October 2002

Nature of Locally Steady Rotor Wakes

Santosh Kini* and A. T. Conlisk†
Ohio State University, Columbus, Ohio 43210

The regions over which steady and unsteady rotor wake patterns exist have been examined numerically for one- and two-bladed rotors. A lifting-line theory is used to model each rotor blade, and a time-stepping vortex method is used to calculate the tip-vortex motion. Tip-vortex geometries for a rotor in hover and vertical climb have been computed. The velocities within the first few turns of the wake have been obtained, and the results indicate a periodic nature of the wake in both time and space. Temporal aperiodicity is observed beyond the first few turns of the tip vortex for hovering rotors, whereas for rotors in sufficient climb the entire wake is steady relative to the blades and both spatially and temporally periodic. Both Euler and Adams–Moulton schemes have been tested for accuracy. The numerical results are shown to be independent of both time step and spatial grid below clearly defined values. Rotor thrust calculations have been performed and the effect of the lower wake on rotor thrust determined. The computed thrust values show some variation because the lower wake remains unsteady. The results for the wake geometry are analyzed and compared to previous predictions and two distinct sets of experimental results.

Nomenclature

A	=	aspect ratio
a_v	=	vortex core radius, m
C_T	=	coefficient of thrust, $T/(\pi\rho\Omega^2 R^4)$
c	=	blade chord, m
N	=	number of blades
R	=	blade radius, m
T	=	rotor thrust, N
u, v, w	=	nondimensional velocity components in the x, y, z directions, respectively
x, y, z	=	nondimensional Cartesian coordinates
Γ	=	nondimensional circulation, $2\pi\Gamma^*/(\Omega R^2)$
Γ^*	=	tip-vortex circulation, $m^2 s^{-1}$
Δt	=	time step or interval, s
$\Delta\psi_b$	=	spatial discretization of the Biot–Savart integral, deg
σ	=	solidity ratio, $N/A\pi$
ψ	=	wake age, deg
ψ_b	=	angle of rotation of blades, deg
Ω	=	angular velocity of rotation of blades, $rads^{-1}$

Introduction

THE occurrence of unsteadiness in rotor wakes and under what conditions it occurs has been a subject of discussion for a long time. The complexity of the wake especially for a large number of blades and the lack of experimental data for the wake beyond a few turns of the rotor make conclusions about the nature of the unsteadiness and when it will occur difficult.[1] Based on the current computations and several previous studies, the behavior of the near wake seems to be far less complicated compared to that beyond a few turns of the tip vortices. The study of the nature of this unsteadiness is important because performance calculations are almost always based on steady or "equilibrium" solutions for the wake.

There have been a number of computational analyses using the vortex method of the type described in this paper. Clark and Leiper[2] presented one of the earliest free wake analyses of rotary wings. They used an iterative procedure, which assumes a basic wake shape and then calculates the velocity field induced by the wake. The computational process was repeated until a converged, steady solution was obtained. This wake was then used to calculate performance characteristics. However, they applied a steady, far boundary condition after only two helical turns and thus could not investigate any unsteadiness occurring below this location.

Landgrebe[3] appears to have been the first to discuss the appearance of unsteadiness in the wake. He attributed the irregularities of the tip-vortex motion in the far wake to either viscous dissipation of the vortex or vortex breakdown, although which effect was responsible was not determined. Kocurek and Tangler[4] found that, relative to the blade-fixed coordinate system, the rotor wake was steady only up to the fourth tip-vortex passage below the reference blade, whereas the rest of the wake never settled down. Also their experimental results show wake expansion in the lower part of the wake, contrary to Landgrebe's[3] assumed contraction. The cause of the wake expansion was believed to be additional inflow caused by recirculation "resulting from the diffused vorticity," and a simple ring vortex was used to model it. The term "recirculation" as used in Ref. 4 does not refer to artificial facility recirculation.

Relaxation methods have also been applied to obtain steady-state configurations. Miller and Bliss[5] utilized a relaxation method in which the solution for the wake is obtained directly by inversion of a linear system of equations arising from a linearized version of the Biot–Savart law governing the vortex motion. In this way no iteration is required, thus saving computer time. Relaxation methods are based on enforcing spatial periodicity as a boundary condition, and the method allows wake convergence without the use of artificial damping. Bagai and Leishman[6] used a relaxation implementation of pseudo-implicit predictor-corrector method with five-point central differencing in space. In both of these papers, no unsteadiness in the far wake was permitted.

The presence of physical irregularities in the wake resulting in significant vortex interactions in hover has been noted previously, and an example of such irregularities has been calculated by Jain and Conlisk.[7] The calculations were motivated by the experimental results presented by Caradonna et al.[8] who show photographs of two tip vortices shed from different blades rolling around each other. A typical experimental result is shown on Fig. 1. Note how the two tip vortices come together and actually wind around each other. In the computations an Adams–Moulton method was used to advance each of the tip vortices; the influence of the inboard sheet on the motion of the tip vortex was shown to be minor and was neglected. The computations presented in Ref. 7 were shown to reproduce the behavior exhibited in the experiments.

Received 16 March 2001; revision received 15 March 2002; accepted for publication 15 April 2002.

*Graduate Research Associate, Department of Mechanical Engineering; currently Mechanical Engineer, Doty Scientific, Inc., Columbia, South Carolina.

†Professor, 206 W. 18th Ave, Department of Mechanical Engineering. Associate Fellow AIAA.

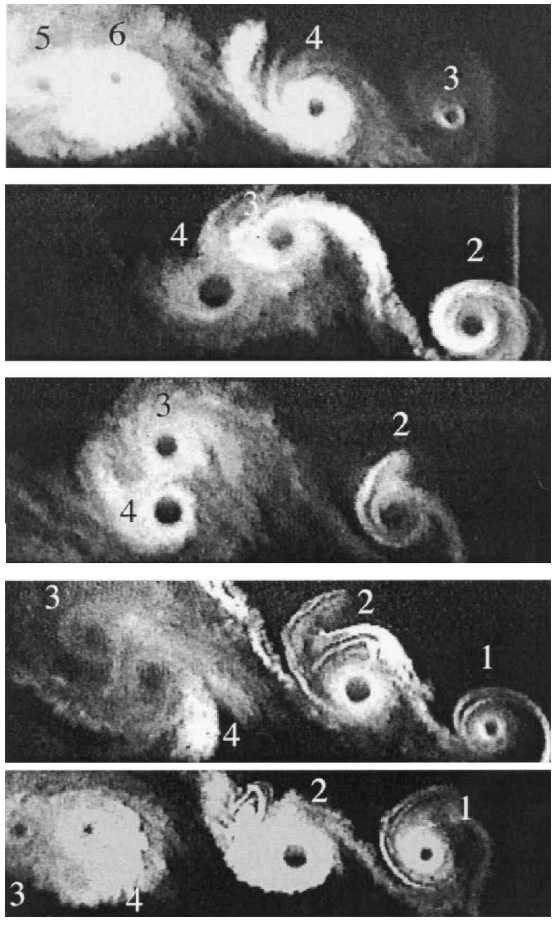

Fig. 1 Sequence of vortex roll up from the individual blades, 9-deg collective pitch, 3.5 fps climb rate.[8] The flow is from right to left.

Similar results have been obtained by Bhagwat and Leishman[9] for a two-bladed rotor. They found irregularities in the fourth turn of the wake using a time-marching technique with five-point central differencing in space and attribute this behavior to "instabilities." No such irregularities were found when two different relaxation schemes were used. The time step used in the time-marching calculations corresponds to a rotor phase angle of 10 deg, and subsequent work by the Bhagwat and Leishman[10] (Figs. 9 and 10 in Ref. 10) shows that these irregularities are caused by numerical error.

In fact, Bhagwat and Leishman[10] suggest that numerical instabilities mimic the physical instabilities, and so it is impossible to tell them apart. For this reason, they suggest that time-marching schemes cannot be used to calculate the dynamics of the rotor wake accurately and claim that the results of Jain et al.[11] exhibit numerical instabilities. In fact, the difference between numerical and physical instabilities is revealed by simply reducing the time step; in the present work numerical instabilities have been observed for all time steps greater than 4 deg, as also shown in Figs. 9 and 10 in Ref. 10. Moreover, the results of Jain et al.[11] are numerically resolved, and so the irregularities seen there are physical in origin. It should be pointed out that the results for the motion of the tip vortex are less sensitive to spatial discretization as discussed later in this paper.

A more complete discussion of the irregularities discussed in this paper and the difficulty of viewing these irregularities as instabilities is given in Jain and Conlisk.[7] In the present paper a conventional, but robust, time-marching method has been applied to the rotor wake problem for one- and two-bladed rotors in hover and vertical climb and also evaluate the extent of their spatial and temporal periodicity. In particular, for hover, the overall thrust is somewhat affected by the unsteadiness in the lower part of the wake, whereas for high climb it is not. The present results are compared with the experimental results of Caradonna et al.[8] and McAlister et al.[12] and the comparison is good.

Numerical Scheme

In the numerical scheme the tip vortex is composed of straight-line vortex segments of equal strength, and the initial condition employed is a smoothly contracting set of helical vortices. At any field point the velocity induced by the vortex line is calculated by Biot–Savart law with a smoothing parameter[13] given by

$$\boldsymbol{U}_V(\boldsymbol{X}, t) = -\frac{\Gamma}{4\pi}\int_C \frac{(\boldsymbol{X}-\boldsymbol{X}')\times \mathrm{d}\boldsymbol{X}'}{(|\boldsymbol{X}-\boldsymbol{X}'|^2+\mu^2)^{\frac{3}{2}}} \tag{1}$$

where $\boldsymbol{X}=(x, y, z)$ is the field point and $\boldsymbol{X}'=(x', y', z')$ the position vector of a point on the vortex and C denotes the space curve occupied by the tip vortices. All lengths in Eq. (1) are normalized by the rotor radius, and the velocity components are normalized by $\Omega R/2\pi$. This means that the dimensionless circulation $\Gamma = 2\pi\Gamma^*/\Omega R^2$, where Γ^* is the dimensional circulation; for all of the calculations except those that are compared with experimental data, $\Gamma = 0.1$. The flow in the vortex is assumed to be a Rankine vortex with radius a_v. The initial core radius normalized on the rotor radius was assumed to be 0.012; this value of the core radius was varied, and it was seen that it had little effect on the results. The core radius a_v is permitted to vary based on volume conservation, and the smoothing parameter based on a Rankine core can be shown to be $\mu = a_v e^{-3/4}$. Each tip vortex is advanced in time by solving

$$\frac{\mathrm{d}\boldsymbol{X}_v}{\mathrm{d}t} = \boldsymbol{U} \tag{2}$$

where $\boldsymbol{X}_v$ is the position vector of a point on the vortex and $\boldsymbol{U}$ is the total velocity induced at that point.

The wake is represented by a few turns of the helix, and beyond a fixed number of turns the wake is represented by a semi-infinite vortex sheet extending to $z=+\infty$. The velocity induced by such a vortex distribution has been determined analytically by Li et al.[14] Various computations were made to test whether the wake geometry depends on the placement of the far-field condition. Calculations were made starting the far boundary condition at the end of 8, 10, and 16 turns. It was found that the wake geometry for the first six turns was unaffected by the placement of the far boundary condition, and for all of the calculations shown here we begin the the far boundary condition after eight turns. To make certain that the results do not depend on the model for the far wake, the far boundary condition of a semi-infinite vortex sheet was replaced by an infinite number of equidistant vortex rings. The solution obtained with this far boundary condition was equivalent to that obtained with the semi-infinite vortex sheet to the numerical error in the Adams–Moulton method. Each blade is represented by a vortex line beginning at the rotor radius of $0.1R$ and ending at R.

The solution is stepped in time using an Adams–Moulton scheme with a Runge–Kutta starting formula. The integral on the right-hand side of Eq. (1) is evaluated at advance points, whereas the integration is carried out using integration points. The integration points are located at the midpoint of each straight-line vortex segment. After every time step each of the advance points is moved to its new location. This method is observed to give better results than when the advance points and integration points coincide.[7] Less accurate schemes such as Euler have also been investigated, and these results are also discussed next.

With each rotor advance the point that was attached at the tip of the rotor is shed into the wake, and the vortex filament formed by joining the point representing the new tip position of the rotor and the new point shed forms a new wake. With the introduction of the new wake, the number of filaments in the wake increases by the number of blades in the computation. To remedy this situation, the vortex point farthest from the blade tip, the old wake, is shed into the far boundary and removed from the computations.

The initial condition was specified as follows. As the solution is stepped in time, the upper part of the wake (3–4 tip-vortex turns) tends to settle down to a spatially and temporally periodic state. Ten to twelve rotor revolutions are required for this state to be attained. The pitch or distance between turns of the tip vortex is not uniform but increases with axial distance: the pitch from the rotor

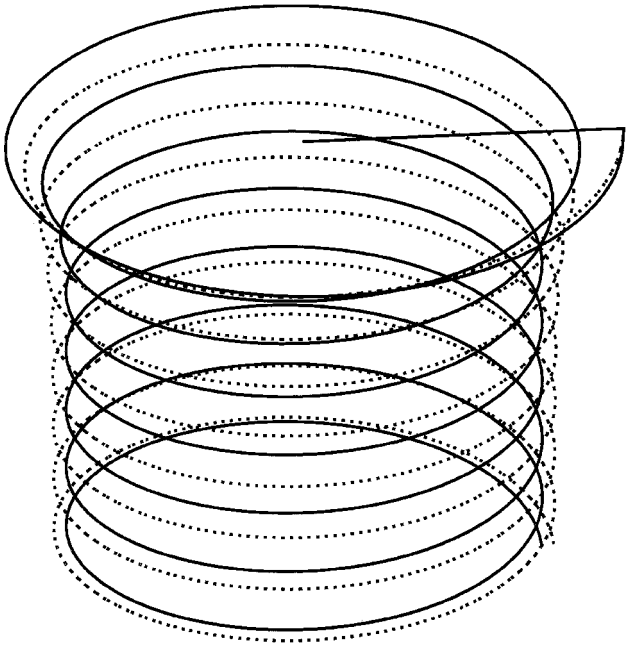

Fig. 2 Comparison between the newly developed initial condition and the conventional wake structure for hover: ——, new initial condition; and · · · ·, conventional wake using Landgrebe's[3] contraction formula.

blade to the first turn is not equal to the pitch between the first and second turn. However the pitch between the second and third turns is nearly equal to the pitch between the first and second turn. The wake geometry from the third turn to the location of the far boundary condition is then extrapolated from this point with the constant value of pitch between the second and third turns. This forms the new initial condition for a wake exhibiting steady, periodic behavior.

The new initial condition is compared to the one obtained by using Landgrebe's[3] contraction formula in Fig. 2 (Ref. 7). It can be observed that the individual turns of the tip vortex in the conventional wake structure are equally spaced although this is not the case with the new initial condition for the first three turns of the tip vortex. The implication is that use of the Landgrebe[3] formula to start the calculation introduces a physical irregularity, which present calculations have shown delays the achievement of a steady state in the first few turns. Both initial conditions lead to the same result ultimately.

Temporal and spatial accuracy has been checked through an extensive set of calculations using time steps and grid spacings between integration points between 16 and 2 deg. These calculations show that for all of the results spatial ($\Delta\psi_b$) and time (Δt) steps of 4 deg each, as used in this paper, are sufficient for four-digit accuracy when compared with the results for $\Delta\psi_b = \Delta t = 2$ deg. It was also found that the wake geometry is much more sensitive to time step than spatial discretization. The tip-vortex strength $\Gamma = 0.10$ has been used throughout, except where noted. It should be pointed out that additional results using the Euler scheme instead of Adams–Moulton indicate that significant numerical error occurs with this scheme for all time steps $\Delta t > 2$ deg; the Adams–Moulton method is much more accurate. Table 1 shows a comparison of Euler and Adams–Moulton schemes with regard to computation time and accuracy. Note that a four-digit accuracy is obtained for $\Delta t = 4$ deg, $\Delta\psi = 8$ deg for the Adams–Moulton method, whereas for the Euler method the same accuracy requires $\Delta t = \Delta\psi = 2$ deg. Thus it takes 4 min and 1 s per rotor revolution to get a four-digit accuracy.

Figure 3 shows the tip-vortex trajectory obtained by Euler and Adams–Moulton schemes for $\Delta t = \Delta\psi_b = 8$ and 16 deg. The result obtained by Adams–Moulton scheme with $\Delta t = \Delta\psi_b = 4$ deg, as mentioned earlier is accurate to four decimal digits, has been laid out in the same plot for comparison. Two points are noteworthy here. First, the Adams–Moulton scheme is far more accurate than the Euler scheme as expected. Secondly, the inaccuracy of the

Table 1 Comparison of Euler and Adams–Moulton schemes

Δt, deg	$\Delta\psi$, deg	E-Time[a]	E-Acc[b]	AM-Time[a]	AM-Acc[b]
2	2	65:33	4	90:55	5
2	4	16:30	3	24:55	5
2	8	04:28	3	07:05	4
4	4	08:12	2	13:05	4
4	8	02:12	2	04:01	4
8	8	01:08	1	02:10	3

[a]E-Time and AM-Time refer to the computation time in minutes: seconds on a SGI R10000 workstation for one rotor revolution using the Euler and Adams–Moulton schemes, respectively.
[b]E-Acc and AM-Acc refer to their corresponding accuracies in terms of the number of decimal digits.

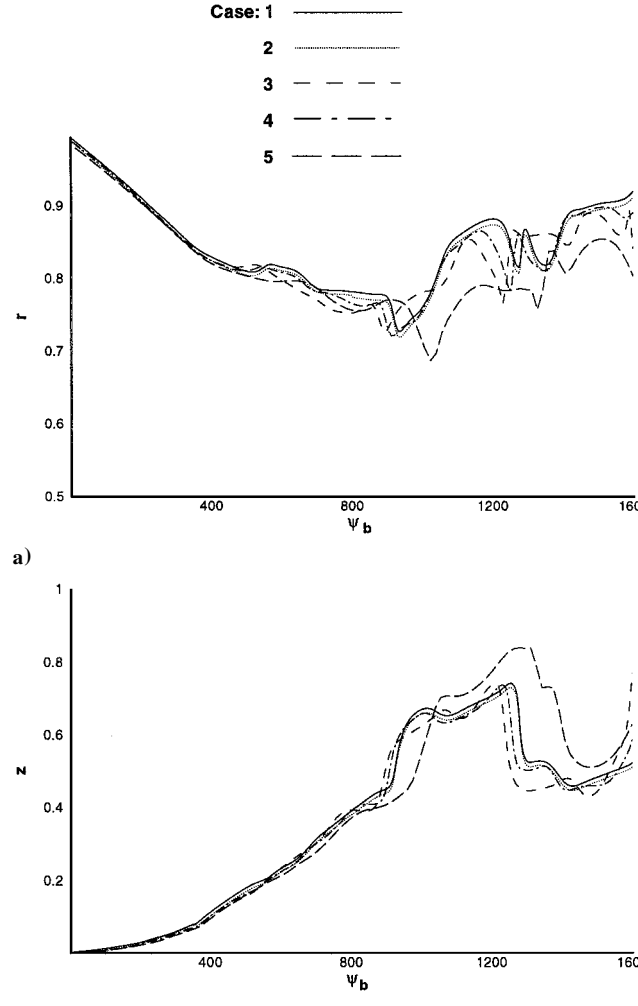

Fig. 3 Tip-vortex trajectory for a single-bladed rotor: a) radial trajectory and b) axial trajectory. Case 1: Adams–Moulton, $\Delta t = \Delta\psi_b = 4$ deg; Case 2: Adams–Moulton scheme, $\Delta t = \Delta\psi_b = 8$ deg; Case 3: Euler scheme, $\Delta t = \Delta\psi_b = 8$ deg; Case 4: Adams–Moulton scheme, $\Delta t = \Delta\psi_b = 16$ deg; and Case 5: Euler scheme, $\Delta t = \Delta\psi_b = 16$ deg.

Euler method is not confined to the lower wake regions only, but begins in the first helical turn of the tip vortex. Thus, on using the Adams–Moulton method with the proper discretization ($\Delta t = 4$ deg, $\Delta\psi_b = 4$ deg or even 8 deg) extremely accurate results are obtained for the entire wake (Table 1). These results indicate that numerical instability is not the source of irregularities in the lower wake as suggested by Bhagwat and Leishman.[10]

Results

Tip-Vortex Geometry and Spatial and Temporal Periodicity

As mentioned earlier, a spatially and temporally periodic solution was obtained for the rotor wake geometry within the first few turns

of the rotor for all calculations performed for hover. Beyond approximately three turns for a one-bladed rotor, the tip vortices looped around without showing temporal or spatial periodicity. This lack of periodicity is shown in Fig. 4 for a single-bladed rotor in hover after four revolutions of the blade. Here, the new initial condition was used to start off the computation.

Figure 5a compares the new initial rotor wake geometry in hover with that after two revolutions of the blade. The wake structures are identical exhibiting total spatial and temporal periodicity. If instead of the new initial condition the conventional wake structure was taken as the initial condition and evolved in time, a comparison as shown in Fig. 5b results. Although the results show no sign of spatial or temporal periodicity, it will settle down subsequently to the wake in Fig. 5a. Thus, starting off with the new initial condition hastens the approach to the steady state although using the conventional initial condition does not inhibit the ability to predict rotor wake periodicity.

Consider two points ***P*** and ***Q*** in the wake as defined in Fig. 6. These points are 15% of the rotor radius below the rotor disk at half-span and are fixed in the laboratory coordinate system. The azimuthal locations of these points are 0 and 180 deg, respectively. Velocity components induced at these points for a single-bladed rotor in hover are shown in Fig. 7. Each velocity component is spatially and temporally periodic with period 360 deg; also both points are within the region where the flow is steady relative to the blade.

Figure 8 shows the wake of a two-bladed rotor in hover. Only the first two turns of the tip vortex from each blade show temporal and spatial periodicity. Thus, if we increase the number of blades in the rotor the extent of spatial and temporal periodicity, in terms of tip-vortex turns from each blade, is reduced. Figure 9 shows the variation in velocity at a point within the wake of a two-bladed rotor in hover. The time period for each of the three velocity components has been reduced by half compared to Fig. 7 (single-bladed rotor) as expected. Thus, the time period will be reduced as the number of blades is increased. On the other hand, if we move down the

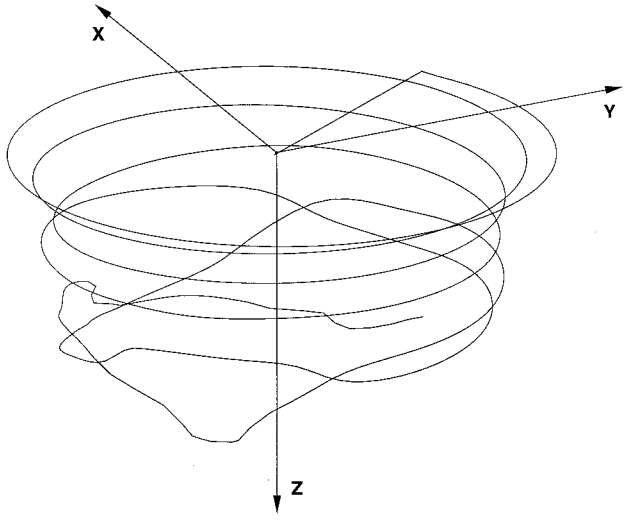

Fig. 4 Wake of a single-bladed rotor in hover after four revolutions of the blade using the new initial condition.

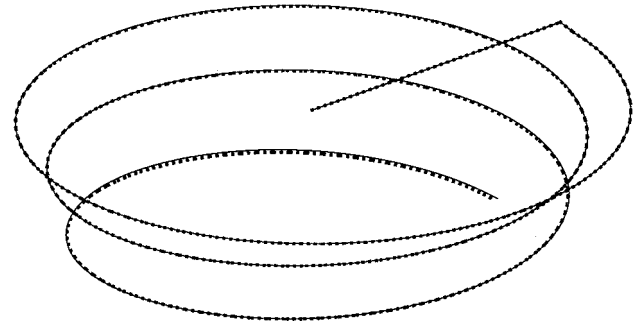

a)

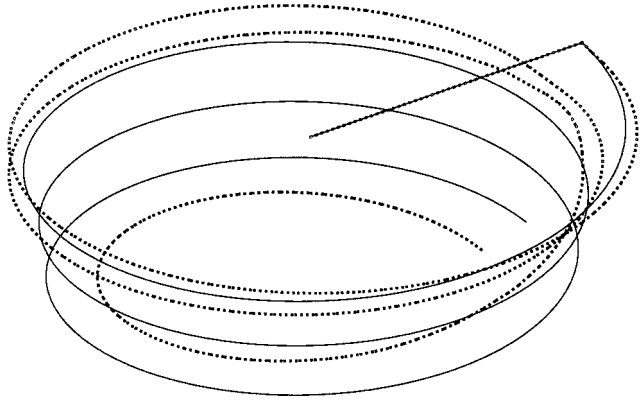

b)

Fig. 5 Comparison between rotor wakes in hover at different times a) using the new initial condition and b) using conventional wake initial condition[7]: ——, initial condition; and · · · ·, after two revolutions of the rotor blade. The conventional initial condition case eventually reaches steady state but only after 14–15 revolutions, compared with 10–12 with the new initial condition.

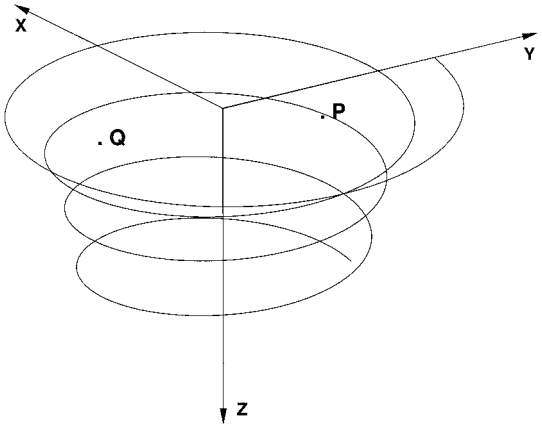

Fig. 6 Location of the points *P* and *Q* at which the velocity components are evaluated.

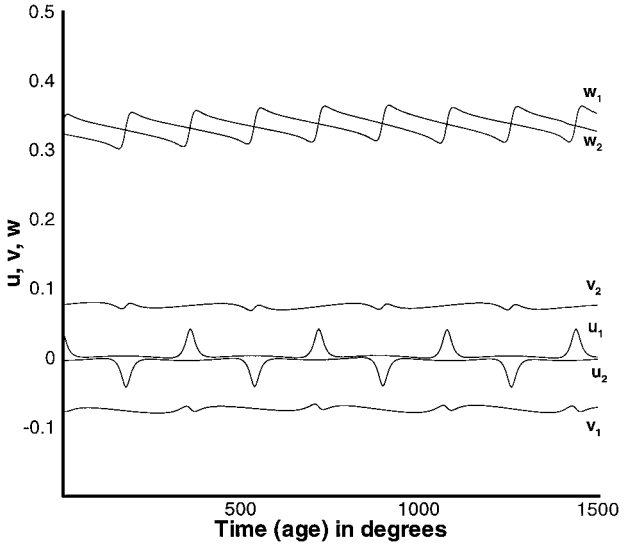

Fig. 7 Velocities induced at diametrically opposite points within the wake of a single-bladed rotor. Velocities with suffix 1 are those induced at point *P*, whereas the velocities with suffix 2 are induced at point *Q*.

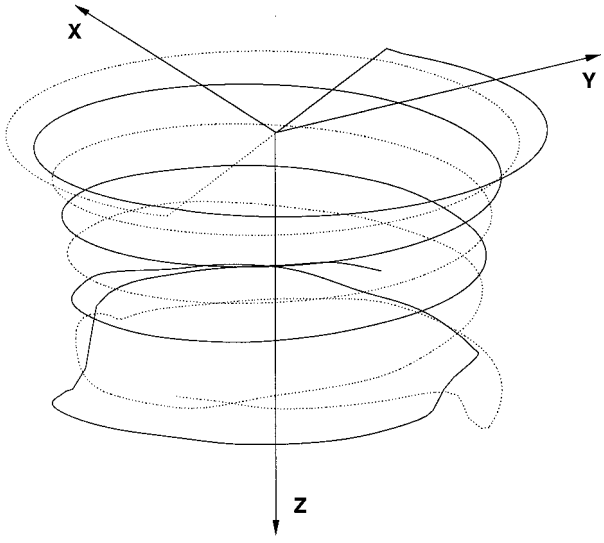

Fig. 8 Wake of a two-bladed rotor in hover after four revolutions of the rotor blades, using the new initial condition: ——, blade-1; and · · · ·, blade-2.

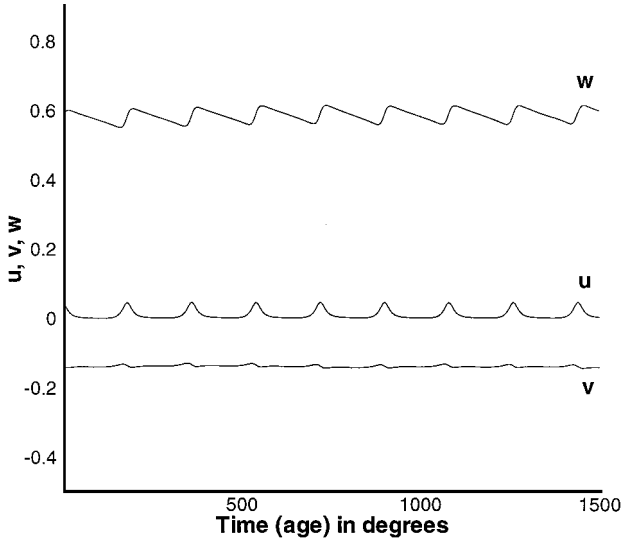

Fig. 9 Velocities induced at a point *P* (Fig. 2) within the wake of a two-bladed rotor in hover.

wake to a point P', which is one blade radius below the rotor plane at half-span and in the unsteady region, the velocity pattern shown in Fig. 10 is obtained. No sign of temporal periodicity is exhibited here.

The wake geometries at several points within the cycle for a hovering two-bladed rotor are shown in Fig. 11. Note that the geometries at $\psi = 180$ and 540 deg are identical, and so are those at $\psi = 360$ and 720 deg, displaying total spatial and temporal periodicity.

Results were also calculated for a high-climb case, and the results are presented in Fig. 12. In high climb it appears that the resulting additional downwash prevents the vortices lower down in the wake from interacting with each other. Here the climb rate is 5% of the tip speed. The entire wake is spatially and temporally periodic; this is also depicted by the velocity pattern at point P within the rotor wake in Fig. 13.

The nonperiodic nature of the wake farther downstream for a rotor in hover is in agreement with the experiments conducted by Kocurek and Tangler[4] as discussed earlier. Specifically, it was observed that for certain sets of parameters the fourth turn of the tip vortex was actually further downstream than the fifth. This occurence was also observed in the experiments carried out by Light.[15]

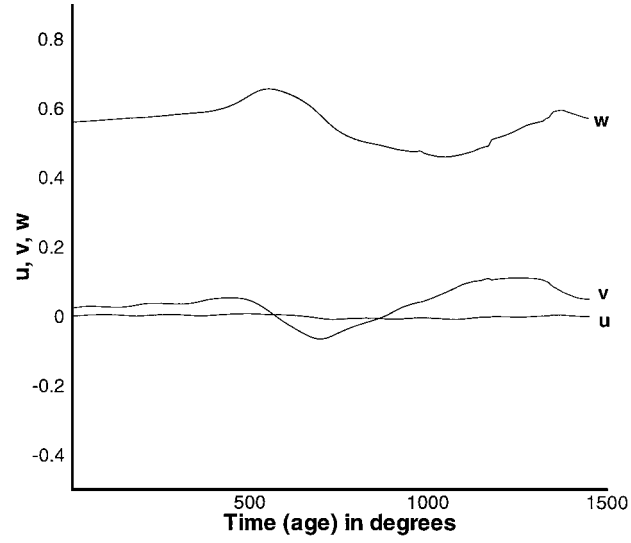

Fig. 10 Velocities induced at a point P' in the unsteady region of the wake of a two-bladed rotor in hover.

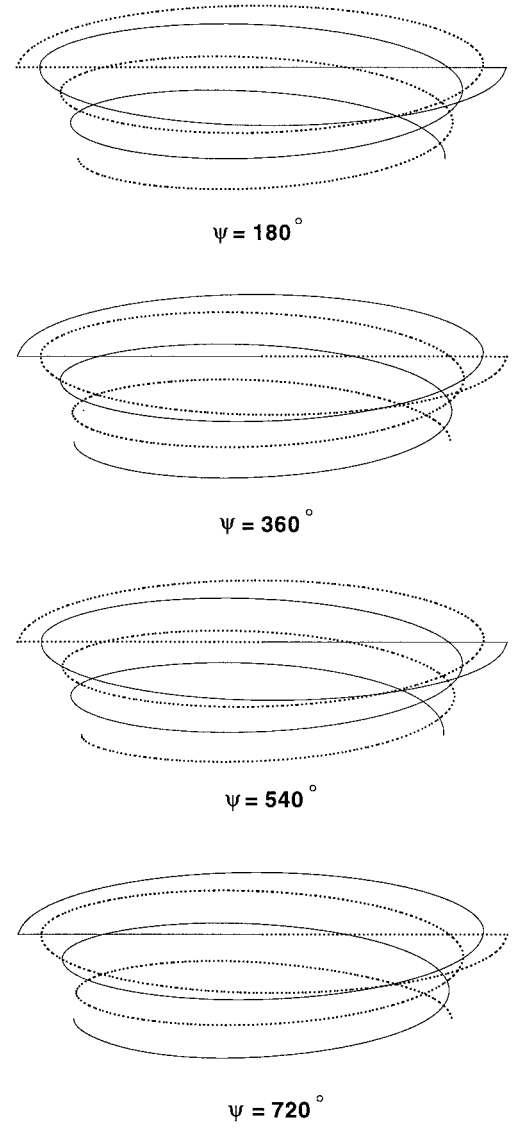

Fig. 11 Two-bladed rotor wake geometries in hover showing spatial and temporal periodicity: ——, blade 1 and tip vortex 1; and · · · ·, blade 2 and tip vortex 2.

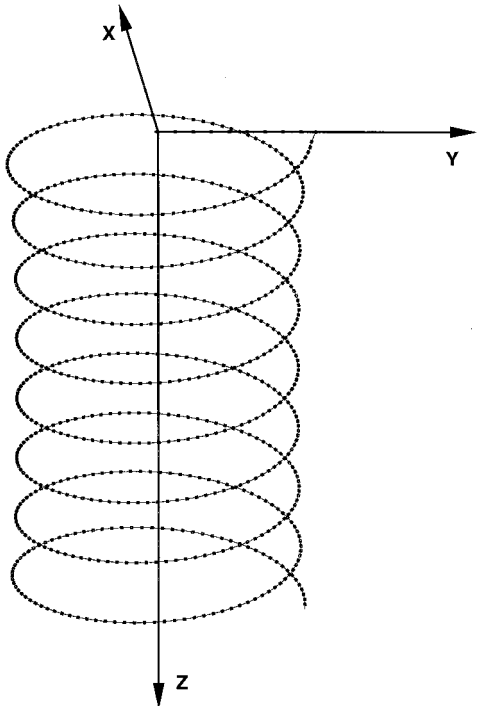

Fig. 12 Wake of a single-bladed rotor in climb. The rate of ascent is 5% of tip speed: ——, initial condition; and · · · ·, after two revolutions of the rotor blade.

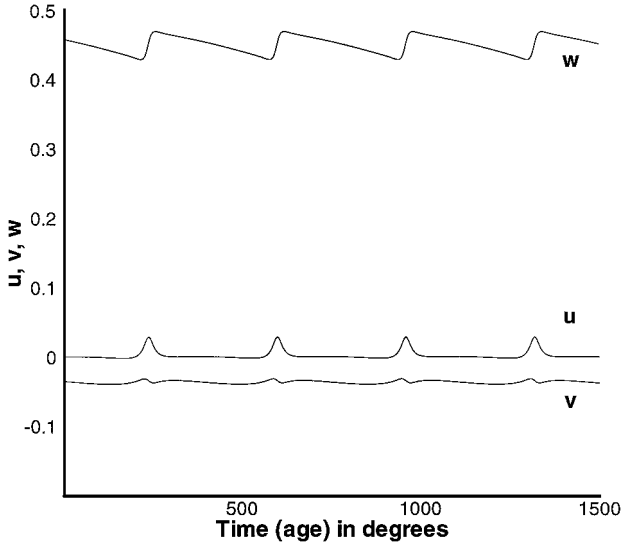

Fig. 13 Velocities induced at point *P* of Fig. 6 within the wake of a single-bladed rotor in climb.

Rotor Thrust

Rotor-thrust calculations were performed for one- and two-bladed rotors in hover and climb. The thrust coefficient is given by

$$\frac{C_T}{\sigma} = \left(\frac{A}{N\pi}\right)\int_0^1 w^2 r\, \mathrm{d}r \tag{3}$$

where w is the nondimensional velocity induced on the blade in the z direction and A is the aspect ratio of the blades (taken as 13.67 for the present computations). r is the radial distance nondimensionalized by rotor radius R. To compute the rotor thrust, we numerically evaluate the integral in Eq. (3) by the trapezoidal rule. Twenty-four azimuthal locations were used with 50 points in each radial direction. The results agreed to four digits with those obtained using 48 azimuthal locations and 100 points in the radial direction.

Table 2 Experimental parameters in the computation[8]

Parameter	Value
R	1.04 m
Ω	188.4 rad/s
c	0.076 m
N	2
a_v	0.0127 m
Γ^*	4.0 m^2/s

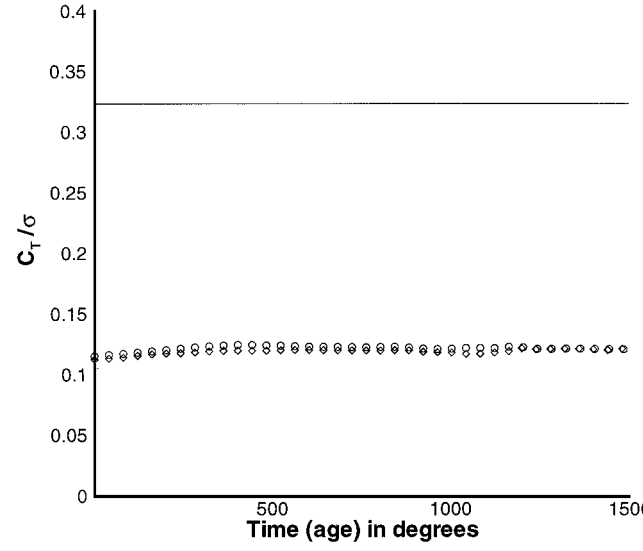

Fig. 14 Variation of C_T/σ in time. Data for one-bladed rotor in hover are represented by o and for two-bladed rotor in hover by ◇ and for climb (5% of tip speed) by ——.

Figure 14 shows the variation of C_T/σ on single-bladed and two-bladed rotors in hover and on a single-bladed rotor in rapid vertical climb (5% of tip speed). The maximum variation of C_T/σ for hover was found to be 7.5% for the single-bladed rotor and 8.24% for the two-bladed rotor. The early time behavior of C_T/σ is not as a result of an initial transient because the first several turns of the tip vortex are steady for both the one- and two-bladed rotor. This indicates that the rotor thrust, although primarily caused by the first three or four turns of the tip vortex, is affected somewhat by the unsteadiness in the lower part of the wake. For rapid vertical climb C_T/σ is a constant throughout.

The computed tip-vortex trajectories were compared with experimental data from Caradonna et al.[8] The experimental parameters are presented in Table 2. Figure 15 shows that the computed trajectories (r and z) are in good agreement with the experiments, and, in particular, are better than previous comparisons.[7] The r and z trajectories in the experimental results for the two blades are not the same, that is, they are not symmetric, unlike the computed result. This could be attributed to dissimilar attack angles or dissimilar blades leading to different strengths of tip vortices.

The phenomena of vortex roll up, as seen in experiments conducted by Caradonna et al.[8] (Fig. 1), are also observed in the present computations, as shown in Fig. 16. The sequence of the computed roll-up process matches with the sequence in the experiments shown in Fig. 1. Moreover, the computed results indicate that vortex rollup occurs many times and thus is a temporally periodic process.

Velocity Distribution Across the Tip Vortex

The velocity field around and across the tip vortex of a single rigid blade was computed and compared with experiments conducted by McAlister.[12] Velocities induced by the entire field were computed at vertical cuts through the tip vortex at $\psi = 30$, 60, and 100 deg. The coordinate system for the experiments is shown in Fig. 17. The vertical velocity induced across the tip vortex is shown in Figs. 18–20 for $\psi = 30$, 60, and 100 deg, respectively. The corresponding

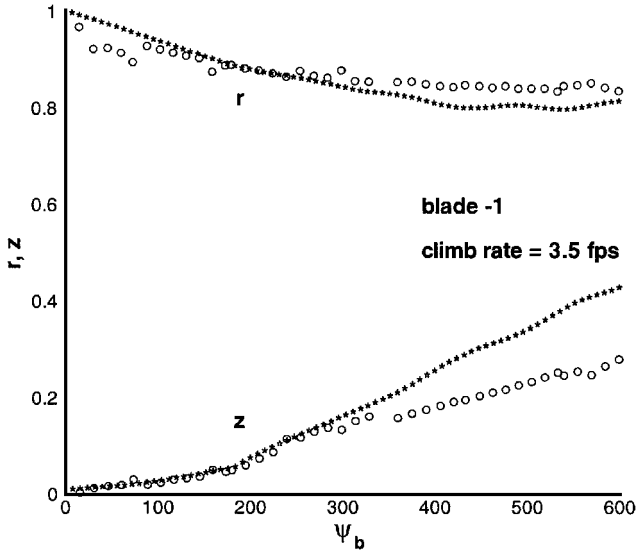

Blade-1

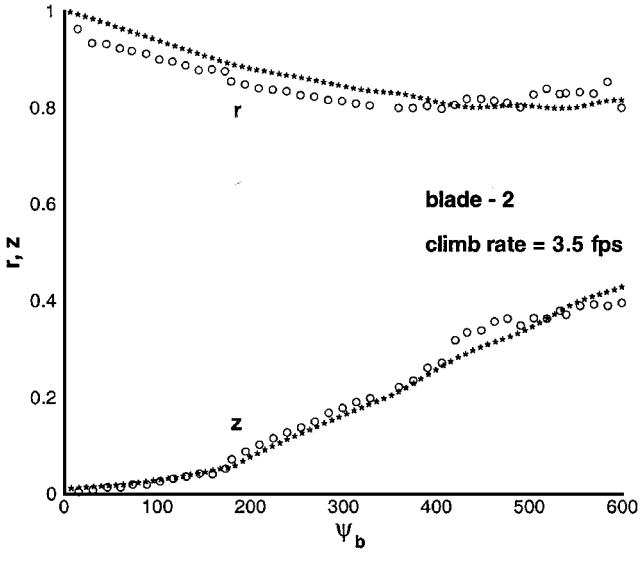

Blade-2

Fig. 15 Comparison of experimental and computational trajectories (r and z) of the tip vortex. Experimental data[8] are represented by o and computational data by ∗.

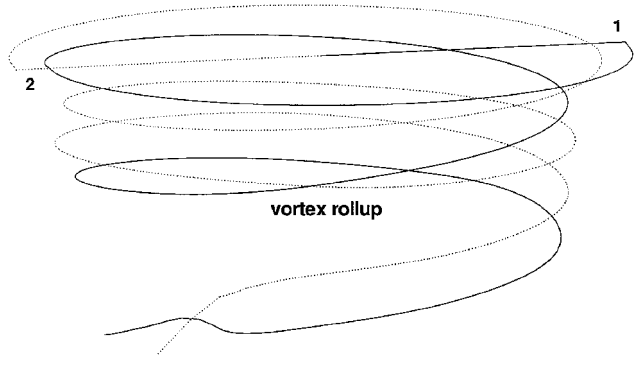

Fig. 16 Computed roll-up process for a two-bladed rotor.

horizontal velocity distribution is shown in Figs. 21–23. All parameters used in the computations, such as circulation and core radius, were obtained directly from experiments. The computations involve no adjustable constants.

Although the computed results agree well with the experiments, it is observed in Figs. 18–20 that the computed results have symmetric peaks of velocity across the tip vortex, but this is not the case with the experimental results. The reason for this might be the effect of the

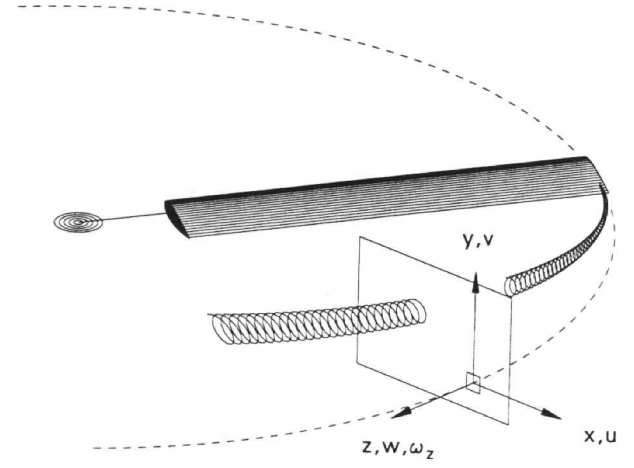

Fig. 17 Coordinate system in experiments conducted by McAlister et al.[12] showing origin on rotor-tip path.

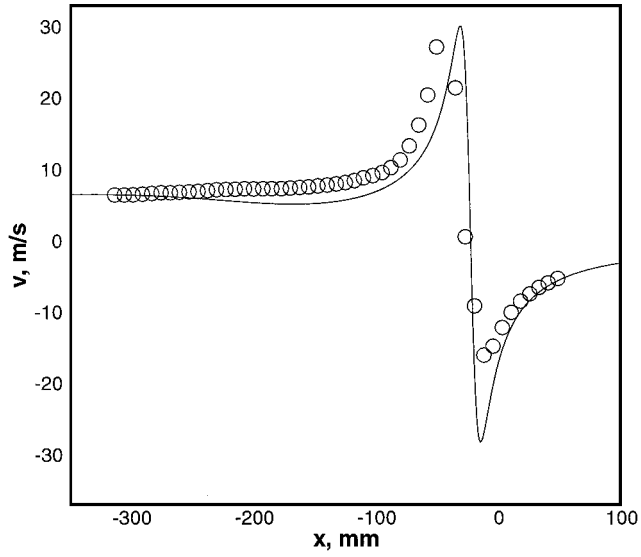

Fig. 18 Vertical velocity across the tip vortex at $\psi = 30$ deg: ——, computed results; and o, experimental results.[14]

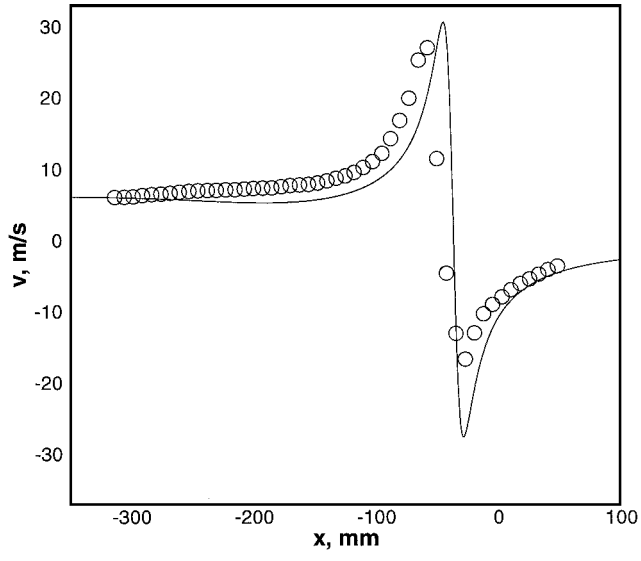

Fig. 19 Vertical velocity across the tip vortex at $\psi = 60$ deg: ——, computed results; and o, experimental results.[14]

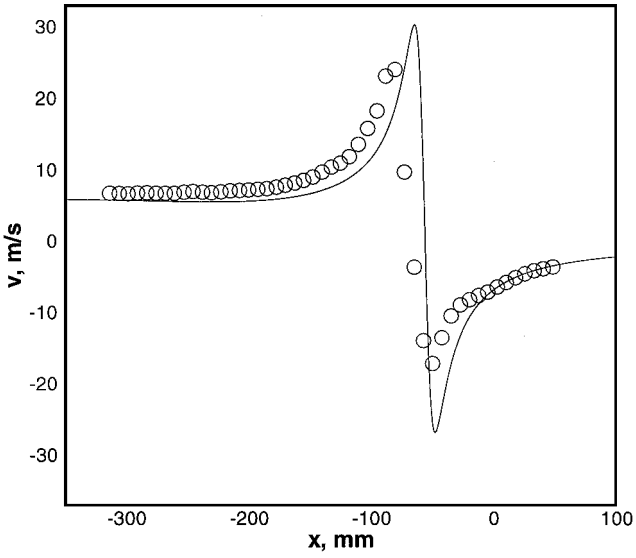

Fig. 20 Vertical velocity across the tip vortex at $\psi = 100$ deg: ——, computed results; and o, experimental results.[12]

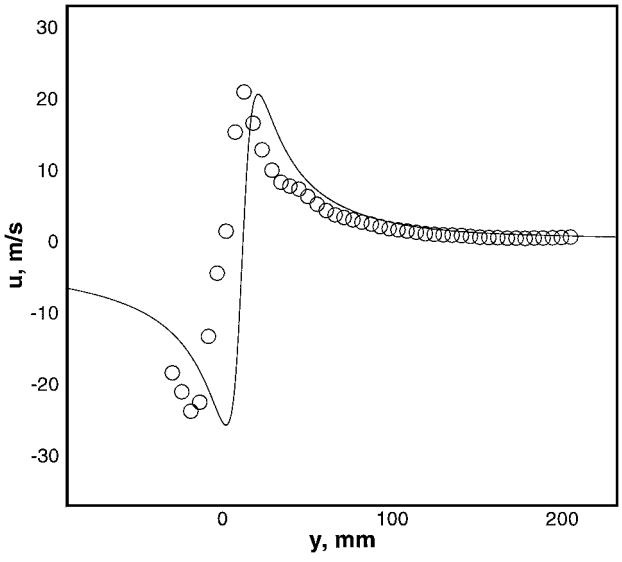

Fig. 21 Horizontal velocity across the tip vortex at $\psi = 30$ deg: ——, computed results; and o, experimental results.[12]

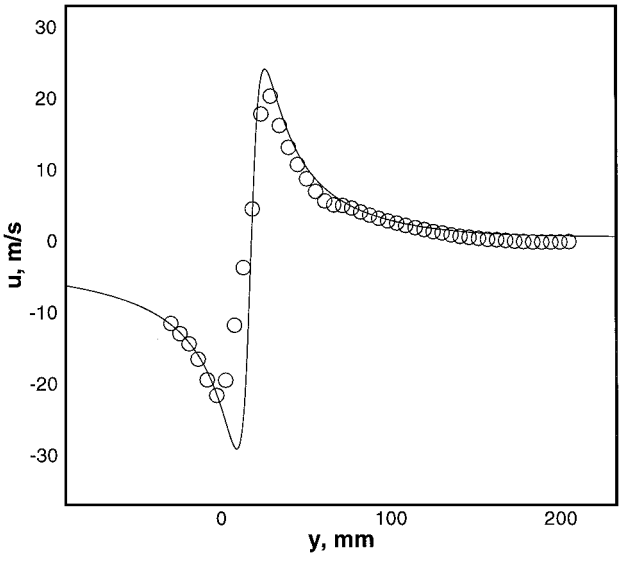

Fig. 22 Horizontal velocity across the tip vortex at $\psi = 60$ deg: ——, computed results; and o, experimental results.[12]

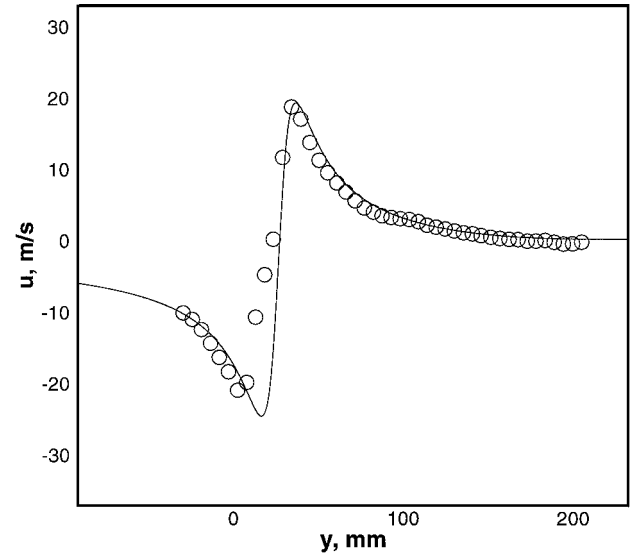

Fig. 23 Horizontal velocity across the tip vortex at $\psi = 100$ deg: ——, computed results; and o, experimental results.[12]

inboard sheet, which has not been accounted for in the computations. The presence of an inboard sheet on one side of the tip vortex causes it to be sheared toward the inside, and thus the magnitude of the inner peak of velocity is greater than that of the outer peak. The influence of inboard sheet will be considered in a future paper.

Conclusions

In this paper we have examined the nature and extent of periodicity of rotor wakes using a time-accurate time-marching technique. Several significant improvements have been made to the code originally developed by Jain and Conlisk.[7]

The reason for the unsteadiness in the far wake seems to be related to the basic behavior of vortices. Two vortices of the same sign and strength will always tend to approach each other. The fact that no nonperiodic phenomena are seen in climb suggests that if the tip vortices are able to stay away from each other the entire flow is steady.

The conclusions are as follows:

1) For hover, a steady, periodic solution is obtained for the first few turns of the tip vortex, whereas the rest of the wake shows no signs of attaining a steady state relative to the blade. This is probably because, in the upper part of the wake, the strong induced effects of the blade-bound circulation and also the entire wake suppress the tendency of the vortices to interact with each other. But these stabilizing effects decrease with axial displacement, and so the lower part of the wake does not settle down to a periodic solution.

2) For high climb the entire wake exhibits a periodic nature in both space and time. The additional velocity in the axial direction as a result of climb forces the tip vortices, in the lower part of the wake, away from each other and into a steady state.

3) The behavior of the lower part of the wake has an effect on rotor thrust. Although most of the thrust is contributed by the first three to four tip vortex turns, a 7–8% variation in thrust is obtained in the calculations reported here.

4) The computed results have been compared with two different sets of experimental data, and the comparison is good.

The tip-vortex circulation and the vortex core radius have been assumed based on existing experimental data. A long-term goal for this research is to couple the tip-vortex model of this paper with a vortex-formation model. This task is a matter for future work.

Acknowledgments

This work was sponsored by the NASA/National Rotorcraft Technology Center Rotorcraft Center of Excellence at Georgia Institute of Technology, Atlanta. The authors are grateful to Ken McAlister for providing experimental data on velocity profiles across the tip

vortex. Thanks are owed also to Rohit Jain for his help and support during the development of the present rotor code.

References

[1]Conlisk, A. T., "The Fluid Dynamics of Rotor Wakes: Theory, Computation and Experiment (Invited)," AIAA Paper 99-3421, June–July 1999.

[2]Clark, D. R., and Leiper, A. C., "The Free Wake Analysis: A Method for the Prediction of Helicopter Rotor Hovering Performance," *Journal of American Helicopter Society*, Vol. 30, No. 1, 1970, pp. 3–11.

[3]Landgrebe, A. J., "The Wake Geometry of a Hovering Rotor and Its Influence on Rotor Performance," *Journal of the American Helicopter Society*, Vol. 14, No. 4, 1972, pp. 3–15.

[4]Kocurek, J. D., and Tangler, J. L., "A Prescribed Wake Lifting Surface Hover Performance Analysis," *Journal of American Helicopter Society*, Vol. 22, No. 1, 1977, pp. 24–35.

[5]Miller, W., and Bliss, D., "Direct Periodic Solutions of Rotor Free Wake Calculations," *Journal of the American Helicopter Society*, Vol. 38, No. 2, 1993, pp. 53–60.

[6]Bagai, A., and Leishman, G., "Rotor Free-Wake Modeling Using a Pseudo-Implicit Technique—Including Comparisons with Experimental Data," *Journal of the American Helicopter Society*, Vol. 40, No. 3, 1995, pp. 29–41.

[7]Jain, R., and Conlisk, A. T., "Interaction of Tip-Vortices in the Wake of a Two-Bladed Rotor in Axial Flight," *Journal of the American Helicopter Society*, Vol. 45, No. 3, 2000, pp. 157–164.

[8]Caradonna, F., Hendley, E., Silva, M., Huang, S., Komerath, N., Reddy, U., Mahalingam, R., Funk, R., Ames, R., Darden, L., Villareal, L., Gregory, J., and Wong, O., "An Experimental Study of a Rotor in Axial Flight," American Helicopter Society, Oct. 1997; also *Journal of the American Helicopter Society*, Vol. 44, No. 2, 1999, pp. 101–108.

[9]Bhagwat, M. J., and Leishman, J. G., "Stability Analysis of Helicopter Rotor Wakes in Axial Flight," *Journal of the American Helicopter Society*, Vol. 45, No. 3, 2000, pp. 165–178.

[10]Bhagwat, M. J., and Leishman, J. G., "Stability, Consistency and Convergence of Time-Marching Free-Vortex Rotor Wake Algorithms," *Journal of the American Helicopter Society*, Vol. 46, No. 1, 2001, pp. 59–71.

[11]Jain, R., and Conlisk, A. T., "Interaction of Tip-Vortices in the Wake of a Two-Bladed Rotor in Hover," *Journal of the American Helicopter Society*, Vol. 45, No. 3, 2000, pp. 157–164.

[12]McAlister, K., Tung, C., and Heineck, J. T., "Devices that Alter the Tip Vortex of a Rotor," NASA/TM-2001-209625,AFDD/TR-01-A-003, Jan. 2001.

[13]Affes, H., Conlisk, A. T., Kim, J. M., and Komerath, N. M., "Model for Rotor Tip-Vortex-Airframe Interaction, Part 2: Comparison with Experiment," *AIAA Journal*, Vol. 31, No. 12, 1993, pp. 2274–2282.

[14]Li, Hui, Burggraf, O. R., and Conlisk, A. T., "Formation of a Rotor Tip-Vortex," *Journal of Aircraft*, Vol. 39, No. 5, 2002, pp. 739–749.

[15]Light, J. S., "Tip Vortex Geometry of a Hovering Helicopter Rotor in Ground Effect," *Journal of American Helicopter Society*, Vol. 38, No. 2, 1993, pp. 34–42.